ATLAS CONF Note

ATLAS-CONF-2020-019

29th May 2020

Measurements of Jet Azimuthal Anisotropies in Pb+Pb collisions at $\sqrt{s_{\mathrm{NN}}}$ = 5.02 TeV

The ATLAS Collaboration

This note describes the measurement of azimuthal anisotropies of jets in Pb+Pb collisions with the ATLAS detector at the LHC. The jets are reconstructed with the anti-k_t algorithm with $R = 0.2$. The azimuthal angles of the jets are measured with respect to the second, third and fourth order event planes as obtained from the ATLAS forward calorimeters. The anisotropies, v_2, v_3, and v_4 are measured as a function of the jet transverse momentum for jets with $71 < p_{\mathrm{T}} < 251$ GeV. The measurement is done as a function of event centrality for 0–10%, 10–20%, 20–40%, and 40–60% centrality intervals. The value of v_2 is found to be larger than zero and v_3 and v_4 are consistent with zero. The values of v_2 and v_3 for jets are found to be consistent with those for charged particles in Pb+Pb collisions at 5.02 TeV as measured by CMS. The values of v_2 are consistent with the jet v_2 measured in 2.76 TeV Pb+Pb collisions by ATLAS, and are found to be lower than v_2 measured by ALICE in central Pb+Pb collisions at 2.76 TeV. This measurement is sensitive to the path length dependence of energy loss of the jets as they traverse the hot nuclear matter, the quark-gluon plasma, produced in Pb+Pb collisions at the LHC.

ATLAS-CONF-2020-019
09 June 2020

1 Introduction

The primary physics aim of the heavy-ion program at the Large Hadron Collider (LHC) is to produce and study the quark-gluon plasma (QGP), the high-temperature state of quantum-chromodynamics (QCD) in which quarks and gluons are no longer confined within protons and neutrons (for a recent review see Ref. [1]). Measurements of jets originating from hard parton scatterings in the early stages of heavy-ion collisions provide information about the short distance scale interactions of high energy partons with the QGP. The overall rate of jets at a given transverse momentum, p_{T}, is found to be reduced by approximately a factor of two with respect to expectations based on pp collisions scaled by the increased partonic luminosity in central Pb+Pb collisions compared to pp collisions [2]. The rates of jets are suppressed up to $p_{\mathrm{T}} \approx 1$ TeV [2]. This suppression can be explained by energy loss of partons propagating through the QGP and the falling shape of the jet p_{T} spectrum. This energy loss from jets is expected to depend on the length of the QGP that the jet travels through. The geometry of the overlap of the two nuclei leads to shorter average path lengths if the jet is oriented along the direction of the collision impact parameter than if the jet is oriented in the perpendicular direction. This should lead to a dependence of the jet yield on the azimuthal angle [3–5]. Recent calculations have shown that realistic modeling of both the jet energy loss and the soft fluctuations are necessary to reproduce the experimental measurements of high-transverse momentum particles [6]. Therefore, it is of interest to study observables that are sensitive to both path length dependence of energy loss and fluctuations of the initial collision geometry [7].

Understanding the path-length dependence of energy loss motivates the study of high momentum anisotropies in large collision systems, such as Pb+Pb collisions, in order to link the angular dependence of jet energy loss with the collision geometry. One key observable is the azimuthal anisotropy of jets. The angular distribution of jets is described via a Fourier expansion:

$$\frac{\mathrm{d}N}{\mathrm{d}\phi} \propto 1 + 2\sum_{n=1}^{n} v_n \cos(n(\phi - \Psi_n)), \tag{1}$$

where Ψ_n is the orientation of the n^{th}-order event plane angle, ϕ is the azimuthal angle of the jet and v_n is the coefficient giving that magnitude of the n^{th}-order modulation. Similar Fourier expansions are often used to describe the azimuthal variation of the yield of soft particles, which is typically associated with hydrodynamic flow (see Ref. [8]). It is important to note that the measurement presented here of the jet v_n is not due to hydrodynamic flow, but rather the correlations of the jet yields with the initial geometry of the collision, which can be obtained through the soft particles in the event. The first measurement of the jet v_2 was done in Ref. [9] for Pb+Pb collisions at $\sqrt{s_{\mathrm{NN}}} = 2.76$ TeV. The measured v_2 values were found to be positive for jets with transverse momentum 45–160 GeV. The v_2 values were found to be smaller in the most central and most peripheral collisions, which is expected. The anisotropy of the initial state is small in the most central collisions, while in the most peripheral collisions there is little energy loss. A measurement by ALICE using jets constructed from charged particles found similar results [10]. Related measurements by CMS and ATLAS have been done with charged particles at high-p_{T} in 5.02 TeV Pb+Pb collisions [11, 12]. Reference [11] reported positive v_2 values for charged particles with p_{T} up to 60–80 GeV. Currently there are no measurements of jet v_2 in $\sqrt{s_{\mathrm{NN}}} = 5.02$ TeV Pb+Pb collisions and no measurements of the higher-order anisotropies, such as v_3 and v_4, of jets in any collision system. Such measurements could provide new information about how the energy loss depends on path length and the initial collision geometry.

The result presented here extends the measurement of jet azimuthal anisotropy to higher-p_{T} and $\sqrt{s_{\mathrm{NN}}} = 5.02$ TeV. Additionally, higher order harmonics, v_3 and v_4, are obtained. The measurement uses

1.72 nb^{-1} of Pb+Pb data collected at $\sqrt{s_{\mathrm{NN}}}$ = 5.02 TeV in 2018. Jets are reconstructed using the anti-k_t [13] algorithm with $R = 0.2$. The small radius jets provide improved position resolution for the estimation of the jet axis compared to larger radius jets, which helps to measure the angular anisotropies. The jets used in this analysis are restricted to $|y| < 1.2$ [1] and $71 < p_{\mathrm{T}} < 251$ GeV. The Ψ_n planes are reconstructed using the transverse energy with $3.2 < |\eta| < 4.9$ and the v_n values are extracted by fitting:

$$\frac{\mathrm{d}N_{\mathrm{jet}}(p_{\mathrm{T}}, \Delta\phi_n)}{\mathrm{d}\Delta\phi_n} \propto 1 + 2v_n \cos(n\Delta\phi_n). \tag{2}$$

$\mathrm{d}N_{\mathrm{jet}}(p_{\mathrm{T}}, \Delta\phi_n)$ is the number of jets for a given p_{T} selection and $\Delta\phi_n$ is the difference in azimuthal angle between the jet azimuthal angle ϕ^{jet} and the Ψ_n plane.

2 ATLAS detector and trigger

The measurement presented in this note is performed using the ATLAS calorimeter, inner detector, trigger, and data acquisition systems [14]. The calorimeter system consists of a sampling liquid-argon (LAr) electromagnetic (EM) calorimeter covering $|\eta| < 3.2$, a steel–scintillator sampling hadronic calorimeter covering $|\eta| < 1.7$, LAr hadronic calorimeters covering $1.5 < |\eta| < 3.2$, and two LAr forward calorimeters (FCal) covering $3.2 < |\eta| < 4.9$. The EM calorimeters are segmented longitudinally in shower depth into three layers with an additional pre-sampler layer. The hadronic calorimeters have three sampling layers longitudinal in shower depth in $|\eta| < 1.7$ and four sampling layers in $1.5 < |\eta| < 3.2$, with a slight overlap in η.

The inner detector measures charged particles within the pseudorapidity interval $|\eta| < 2.5$ using a combination of silicon pixel detectors, silicon microstrip detectors (SCT), and a straw-tube transition radiation tracker (TRT), all immersed in a 2 T axial magnetic field [14]. Each of the three detectors is composed of a barrel and two symmetric end-cap sections. The pixel detector is composed of four layers including the Insertable B-Layer [15, 16]. The SCT barrel section contains four layers of modules with sensors on both sides, and each end-cap consists of nine layers of double-sided modules with radial strips. The TRT contains layers of staggered straws interleaved with the transition radiation material.

The zero-degree calorimeters (ZDCs) are located symmetrically at $z = \pm 140$ m and cover $|\eta| > 8.3$. The ZDCs use tungsten plates as absorbers, and quartz rods sandwiched between the tungsten plates as the active medium. In Pb+Pb collisions, the ZDCs primarily measure "spectator" neutrons that do not interact hadronically when the incident nuclei collide. A ZDC coincidence trigger is implemented by requiring the pulse height from both ZDCs to be above a threshold which is set to accept the signal corresponding to the energy deposition from a single neutron.

ATLAS uses a two-level trigger system. The first, a hardware-based trigger stage named Level-1 is implemented with custom electronics. The next level is the software-based High-Level Trigger (HLT).

[1] ATLAS uses a right-handed coordinate system with its origin at the nominal interaction point (IP) in the center of the detector, and the z-axis along the beam pipe. The x-axis points from the IP to the center of the LHC ring, and the y-axis points upward. Cylindrical coordinates (r, ϕ) are used in the transverse plane, ϕ being the azimuthal angle around the z-axis. The pseudorapidity is defined in terms of the polar angle θ as $\eta = -\ln\tan(\theta/2)$. The rapidity is defined as $y = 0.5\ln[(E + p_z)/(E - p_z)]$ where E and p_z are the energy and z-component of the momentum along the beam direction respectively. Transverse momentum and transverse energy are defined as $p_{\mathrm{T}} = p\sin\theta$ and $E_{\mathrm{T}} = E\sin\theta$, respectively. The angular distance between two objects with relative differences $\Delta\eta$ in pseudorapidity and $\Delta\phi$ in azimuth is given by $\sqrt{(\Delta\eta)^2 + (\Delta\phi)^2}$.

3 Data and Monte Carlo samples

All events included in this analysis are required to contain at least one reconstructed vertex as well as to satisfy detector and data-quality requirements that ensure the detector is in nominal operating condition. The events were selected by the HLT, which was seeded by a L1 jet trigger performing a simple sliding window algorithm to find jet candidates and requiring minimum p_{T} thresholds of 15, 20, and 30 GeV. The HLT jet trigger uses a jet reconstruction algorithm similar to that used in the offline analysis and applies cuts on the minimum transverse energy, E_{T}, of $R = 0.4$ jets of 50, 60, 85, and 100 GeV. The analysis is done in the region of jet p_{T} for which the HLT triggers are above 99% efficient. In addition to the jet triggered sample, a minimum-bias (MB) triggered sample defined by a logical OR of the following two triggers is used: 1) the total energy Level-1 trigger of at least 50 GeV; 2) a veto on the total-energy trigger, plus requirements of a ZDC coincidence trigger at Level-1 and at least one track in the HLT. More details about the jet triggering in heavy-ion collisions can be found in Ref. [17]. Although only a small fraction of Pb+Pb events ($< 0.5\%$) contain multiple Pb+Pb collisions, the anti-correlation between the total transverse energy deposited in the forward calorimeter, $\Sigma E_{\mathrm{T}}^{\mathrm{FCal}}$, and the number of neutrons measured in the ZDC is used to suppress these events.

The overlap area of two colliding nuclei in Pb+Pb collisions is characterized by the total transverse energy deposited in the FCal [18]. This analysis uses four centrality intervals which are defined according to successive percentiles of the $\Sigma E_{\mathrm{T}}^{\mathrm{FCal}}$ distribution obtained in Minimum Bias collisions. The centrality regions used in this analysis, starting at the most central (largest $\Sigma E_{\mathrm{T}}^{\mathrm{FCal}}$) to peripheral (lowest $\Sigma E_{\mathrm{T}}^{\mathrm{FCal}}$) collisions are: 0–10%, 10–20%, 20–40%, and 40–60%.

This analysis uses Monte Carlo (MC) simulations to evaluate the performance of the detector and analysis procedure, and to correct the measured distributions for detector effects. The detector response in all MC samples was simulated using GEANT4 [19, 20]. The Pb+Pb MC sample uses 32×10^6 pp PYTHIA8 dijet events with the A14 ATLAS tune [21] and the NNPDF23LO parton distribution functions [22] that are overlayed with events from a dedicated sample of Pb+Pb data events. This sample was recorded with combination of MB trigger and total energy triggers requiring 1.5 TeV or 6.5 TeV to enhance the number of central collisions. The overlay procedure combines the PYTHIA and data events during the digitization step of simulation. This "MC overlay" sample was reweighted on an event-by-event basis such that it has the same $\Sigma E_{\mathrm{T}}^{\mathrm{FCal}}$ distribution as the jet-triggered data sample to better represent the data used in this analysis.

4 Jet reconstruction and analysis procedure

The jet reconstruction procedures closely follow those used by ATLAS for previous jet measurements in Pb+Pb collisions [2, 9]. Jets were reconstructed using the anti-k_t algorithm [13] implemented in the `FastJet` software package [23]. The jets with $R = 0.2$ were formed by clustering calorimetric "towers" of spatial size $\Delta\eta \times \Delta\phi = 0.1 \times \frac{\pi}{32}$. The energies in the towers are obtained by summing the energies of calorimeter cells at the electromagnetic energy scale [24] within the tower boundaries. A background subtraction procedure was applied that uses the underlying event (UE) average transverse energy density, $\rho(\eta, \phi)$ where the ϕ dependence is due to global azimuthal correlations in the particle production typically referred to as "flow" [25]. The modulation accounts for the contribution of the second, third, and fourth-order azimuthal anisotropy harmonics characterized by values of flow coefficients v_n [12]. The UE is also corrected for η- and ϕ-dependent non-uniformities of the detector response by multiplicative correction factors derived in MB Pb+Pb data.

An iterative procedure was used to remove the impact of jets on ρ and the v_n values. The first estimate of the UE average transverse energy density, $\rho(\eta)$, was evaluated in 0.1 intervals of η excluding those within "seed" jets. In the first subtraction step, the seeds are defined to be a conjunction of $R = 0.2$ jets and $R = 0.4$ track jets. Track jets were reconstructed by applying the anti-k_t algorithm with $R = 0.4$ to charged particles with $p_{\mathrm{T}} > 4$ GeV. The $R = 0.2$ jets have to pass the cut on the value of maximal-over-mean tower energy while the track jets are required to have $p_{\mathrm{T}} > 7$ GeV. The background is then subtracted from each tower constituent and jet kinematics parameters are recalculated. After the first iteration, the ρ and v_n values are updated by excluding regions within $\Delta R < 0.4$ from the newly reconstructed $R = 0.2$ jets with $p_{\mathrm{T}} > 25$ GeV, and track jets. The updated ρ and v_n values are used to update the jet kinematic properties in the second iteration.

Jet η- and p_{T}-dependent correction factors derived in simulations are applied to the jet energy to correct for the calorimeter energy response [26]. An additional correction based on *in situ* studies of jets recoiling against photons, Z bosons, and jets in other regions of the calorimeter is applied [27]. This calibration is followed by "cross-calibration" which relates the jet energy scale (JES) of jets reconstructed by the procedure outlined in this section with the JES in 13 TeV pp collisions [28]. The jet reconstruction in pp collisions is performed without correcting the UE for η and ϕ variation in the detector response and without azimuthal modulation of the UE.

So-called truth jets are defined in the MC sample by applying the anti-k_t algorithm with $R = 0.2$ to stable particles with a proper lifetime greater than 30 ps, but excluding muons and neutrinos, which do not leave significant energy deposits in the calorimeter.

The JES and jet energy resolution (JER) for $R = 0.2$ jets are shown in Fig. 1. They are derived by matching each truth jet to the closest reconstructed and calibrated jet from the MC sample within an angular distance of $\Delta R < 0.15$. The JES and JER are taken to be the mean and standard deviation of the $p_{\mathrm{T}}^{\mathrm{reco}}/p_{\mathrm{T}}^{\mathrm{true}}$ distribution, respectively. The JES differs from unity by approximately 1% at 70 GeV and 2% at 200 GeV; this deviation is due to the isolation cuts used in the determination of the jet calibration and is corrected by the unfolding procedure described below. The JES has no significant centrality dependence. The JER improves with increasing p_{T} and going from central to peripheral collisions. The JES has a small dependence on $\Delta\phi_2$, with variations up to approximately 0.5% between in-plane and out-of-plane jets. The JER also shows a small dependence on $\Delta\phi_2$, with the resolution of in-plane jets up to 0.3% larger than out-of-plane jets. Jets in this analysis are selected with rapidity $|y| < 1.2$ to minimize the JES dependence on $\Delta\phi_2$.

This analysis uses the event plane method for measuring the jet v_n as has been previously used in ATLAS measurements [9, 12, 29]. The event plane angles Ψ_n are determined by the azimuthal distribution of transverse energy in the forward calorimeters as described in Ref. [12].

The event plane resolution is determined by comparing the event plane angles determined by the positive and negative rapidity sides of the FCal, and is used to correct the measured v_n values as described in Ref. [30]. The jet yield is measured as a function of the azimuthal angle of the jet with respect to the event plane angles, $\Delta\phi_n = |\Psi_n - \phi|$, in bins of p_{T} and centrality.

To correct for detector effects, the $\Delta\phi_n$ distributions are unfolded before v_n harmonic fitting with a two dimensional Bayesian unfolding [31] using the `RooUnfold` package [32]. The unfolding is done in p_{T} and $\Delta\phi_n$. For each centrality and order n, a response matrix is filled using truth-reconstructed pairs of jets from the MC overlay sample. Truth jets are matched to the closest reconstructed jet with $\Delta R < 0.15$. The two-dimensional unfolding allows for corrections due to jet energy scale and resolution and jet angular resolution effects, including dependencies of the jet energy scale and resolution on the jet angle with

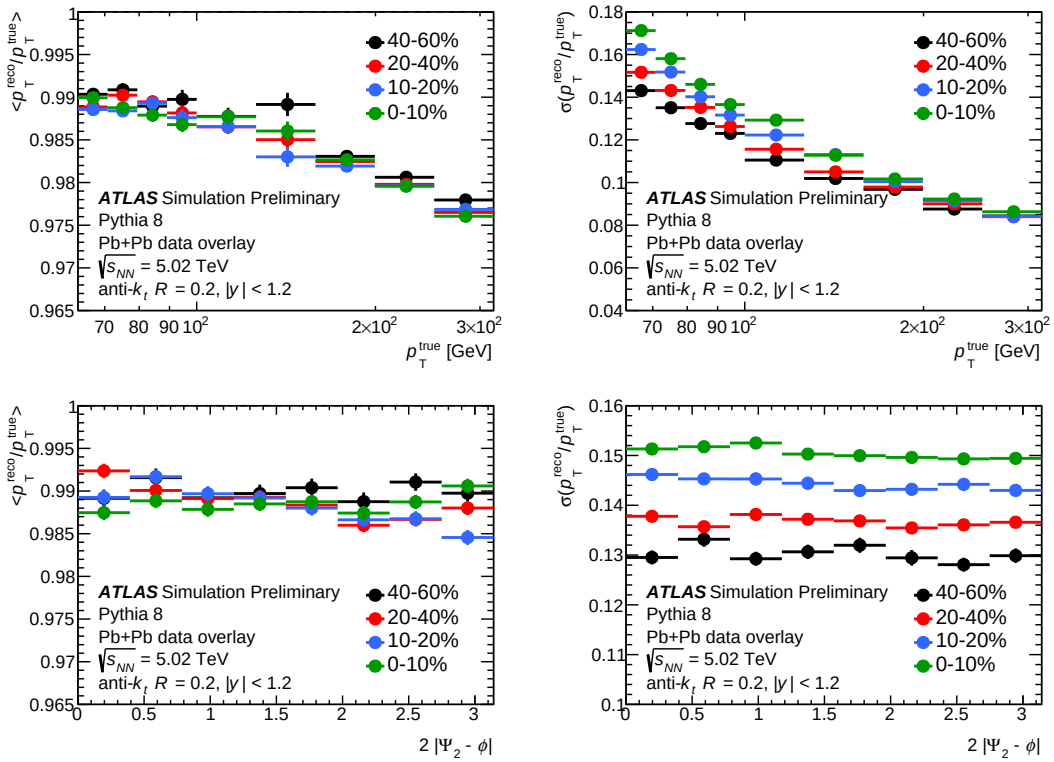

Figure 1: The JES (left) and JER (right) for $R = 0.2$ jets in Pb+Pb collisions as a function of p_{T} (top) and $\Delta\phi_2$ (bottom) for centrality selections of 0–10%, 10–20%, 20–40% and 40–60%.

respect to the event plane. Any difference in the modeling of the JES and JER dependence on the angle with respect to the event plane between data and MC is expected to be small due to the overall small size of the effect seen in MC and is therefore not assessed as an uncertainty. The response matrix is reweighted in truth p_{T} and $\Delta\phi_n$ by the ratio of reconstructed data to reconstructed MC to better represent the data. The unfolding is performed using three iterations, which has been selected to minimize the statistical uncertainty and relative bin migration after each iteration.

For each selection in p_{T}, centrality and harmonic value n, unfolded $\Delta\phi_n$ distributions are fit to extract the v_n values. The fit function is:

$$A(1 + 2v_n \cos(n\Delta\phi_n)) \tag{3}$$

where the overall normalization A and the value of v_n are the free parameters in the fitting procedure. The measured v_n values are then corrected for the event plane resolution. This is a multiplicative correction of $\frac{1}{\mathrm{Res}(\Psi_n)}$, with values of $\mathrm{Res}(\Psi_n)$ ranging from 0.78–0.94 for Ψ_2, 0.45–0.7 for Ψ_3, and 0.27–0.49 for Ψ_4. In addition to the v_n measurements differential in jet p_{T}, the values are also obtained in an inclusive p_{T} bin for jets with $71 < p_{\mathrm{T}} < 251$ GeV, following the same procedure as used in the differential measurement.

5 Systematic Uncertainties

The systematic uncertainties in this measurement arise from: the JES and JER, the unfolding procedure, and the bias of the event plane by a forward-produced jet correlated with the jet of interest. For each

uncertainty component the entire analysis procedure is repeated with the variation under consideration and the uncertainties contributions are added in quadrature to form the final systematic uncertainties on the measurement.

The systematic uncertainty on the JES has five parts. First, centrality-independent baseline component that is determined from *in situ* studies of the calorimeter response of jets reconstructed with procedure used in 13 TeV pp collisions [33, 34]. The second, centrality-independent component accounts for the relative energy scale difference between the jet reconstruction procedures used in this note and that in 13 TeV pp collisions [28]. Potential inaccuracies in the MC sample in the description of the relative abundances of jets initiated by quarks and gluons and of the calorimetric response to quark and gluon jets are accounted for by the third component. The fourth, centrality-dependent, component accounts for a different structure and possibly a different detector response of jets in Pb+Pb collisions that is not modeled by the MC. It is evaluated by the method used for 2015 and 2011 data [28] that compares calorimeter p_{T} and the sum of the transverse momentum of charged particles within the jet in data and MC samples. The size of the centrality-dependent uncertainty on the JES reaches 0.8% in the most central collisions. The systematic uncertainties from JES discussed above are derived for $R = 0.4$ jets. The last component does not depend on collision centrality and it accounts for the potential difference in uncertainties between $R = 0.4$ and $R = 0.2$ jets. The uncertainty is assessed by comparing the ratio of p_{T} for R = 0.2 to R = 0.4 jets between data and MC. The size of this uncertainty on the JES is approximately 1%. Each component is varied separately by ± 1 standard deviation in MC samples, applied as a function of p_{T} and η, and the response matrix is recomputed. The data are then unfolded with the modified matrices.

The uncertainty due to the JER is evaluated by repeating the unfolding procedure with modified response matrices, where an additional contribution is added to the resolution of the reconstructed p_{T} using a Gaussian smearing procedure. The smearing factor is evaluated using an *in situ* technique in 13 TeV pp data that involves studies of dijet energy balance [35, 36]. Further, uncertainty is included to account for differences between the tower-based jet reconstruction and the jet reconstruction used in analyses of 13 TeV pp data, as well as differences in calibration procedures. Similarly to the JES, an additional uncertainty on JER accounting for differences between $R = 0.2$ and $R = 0.4$ jets is added. The resulting uncertainty from the JER is symmetrized.

The unfolding uncertainty was determined by not applying the reweighting of the response matrix. The unweighted response matrix was used to unfold the $\Delta\phi_n$ distributions and the results were fitted to obtain new v_n results. The difference from the nominal unfolding result was symmetrized and taken as the systematic uncertainty contribution. The precision of the unfolding is in some cases impacted by the available number of MC events. This is evaluated by resampling the MC to generate alternate response matrices and this uncertainty is included in the statistical uncertainty bars.

The uncertainty on the event plane resolution as determined in Ref. [29] was found to be negligible as compared to other uncertainties and is not included. However, it is possible for a jet correlated with the jet of interest to bias the event plane if some of its energy is in the FCal. An estimate of the size of this effect was determined from the MC samples. The MC samples are produced without a correlation between the dijets in Pythia8 and the Ψ_n angles in the data event. Therefore, the measured v_n of jets coming from the Pythia event should be zero. A non-zero v_n could be caused by some events having their event plane determination biased by a MC jet. This effect is expected to be most significant in peripheral collisions, where the total $\Sigma E_{\mathrm{T}}^{\mathrm{FCal}}$ is smallest and therefore the contribution from the jet will cause a larger bias. The size of this effect in data is estimated by the v_n values found in the MC sample and it is taken as a systematic uncertainty. This effect only increases the measured v_2 value and therefore is taken as a single

sided uncertainty on v_2. However, the uncertainty on v_3 and v_4 is found to have both negative and positive components and therefore is symmetrized.

The total systematic uncertainties on the v_n values are summarized in Fig. 2. The systematic uncertainties are currently limited by statistical fluctuations from the MC in the response matrices which require additional analysis to separate from the systematic variations. In general the unfolding and event plane biases are the largest components to the uncertainties on the v_n values. The systematic uncertainties are determined using the same procedure for the inclusive jet p_{T} bin, 71–251 GeV. Here the uncertainties related to bin migration, namely the JES, JER, and unfolding, are small and the event plane bias uncertainty dominates.

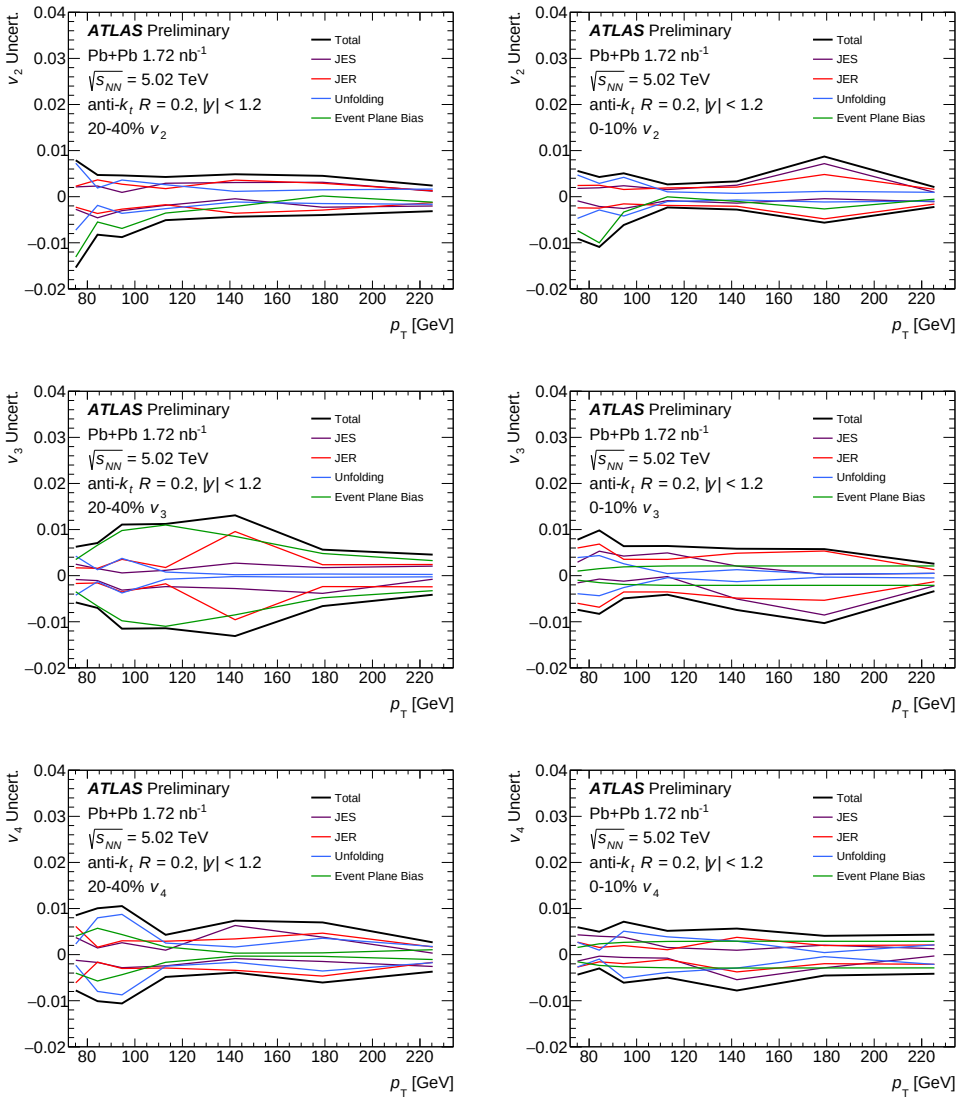

Figure 2: The systematic uncertainties on v_2 (top), v_3 (middle), and v_4 (bottom) for 20–40% (left) and 0–10% Pb+Pb collisions (right) as a function of p_{T}. Each panel shows the total systematic uncertainty as well as the size of the uncertainty from each of the sources, namely the JES, JER, unfolding, and event plane bias.

6 Results

Figures 3 and 4 show the angular distribution of jets with respect to the Ψ_2 and Ψ_3 planes, respectively, for jets with $100 < p_{\mathrm{T}} < 126$ GeV for the four centrality selections in this analysis. For the Ψ_2 dependence, in all cases there are more jets in-plane than out-of-plane (though the significance is smaller in the 0–10% most central collisions). For the Ψ_3 dependence, there is no clear angular dependence of the jet yields.

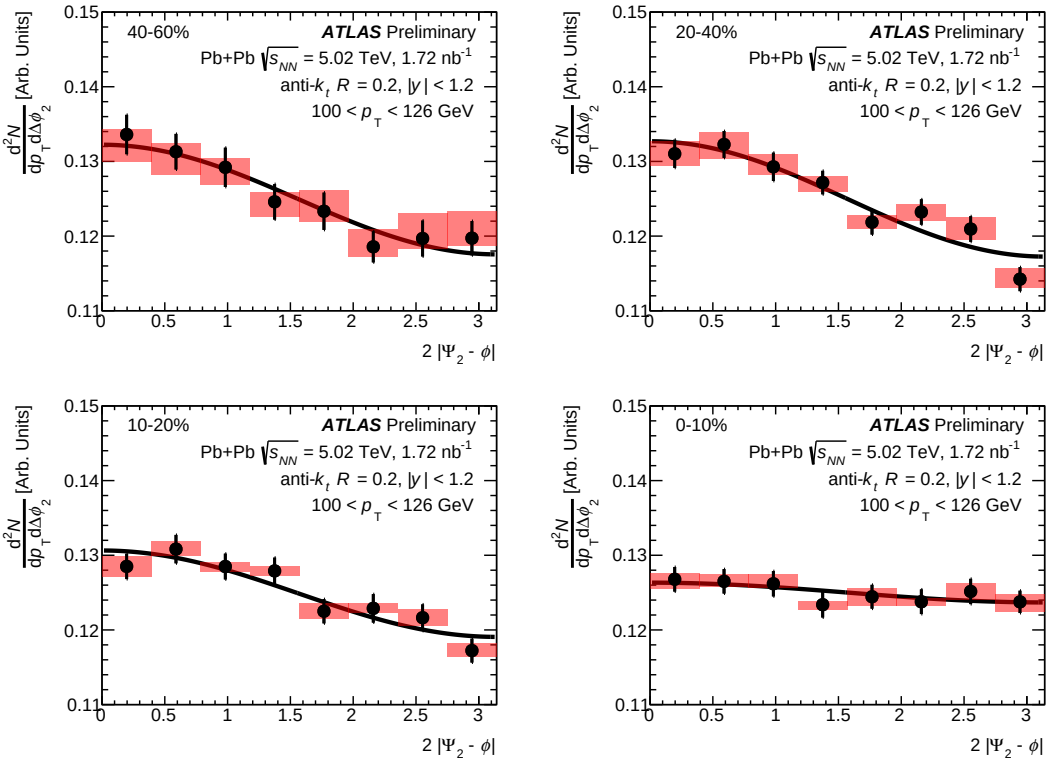

Figure 3: Angular distribution of jets with respect to the Ψ_2 plane for jets with $100 < p_{\mathrm{T}} < 126$ GeV for (from top left): 40–60%, 20–40%, 10–20%, and 0–10% central Pb+Pb collisions. The vertical bars show the statistical uncertainties and the boxes show the systematic uncertainties. The fits are to the function in Eq. 3.

Figure 5 shows the v_2 values as a function of centrality for the jets with p_{T} from 71–251 GeV. The v_2 values are positive for all the centrality and p_{T} selections measured. The v_2 values are measured to be approximately 1% to 5%. The values are larger in peripheral and mid-central collisions than in the most central collisions as expected from the collision geometry, however the uncertainties are large which limits the significance of the centrality dependence. The centrality dependence of the v_3 and v_4 values are shown in Figure 6. Here the uncertainties are larger than those for the v_2 values and no significant v_3 or v_4 is observed in this measurement.

In Figure 7 the v_2 values measured in this analysis are compared to the jet v_2 values at $\sqrt{s_{\mathrm{NN}}} = 2.76$ TeV from both ATLAS [9] and ALICE [10] for the 0–10% and 20–40% centrality selections. The ATLAS v_2 values at the lower collision energy are consistent in both centrality ranges with those measured here in both centrality classes. The ALICE v_2 values are consistent with the values measured here in the 20–40% centrality class but are significantly higher than the values measured here in the 0–10% centrality class. The ATLAS measurement at 2.76 TeV uses jets reconstructed in a nearly identical manner to those measured

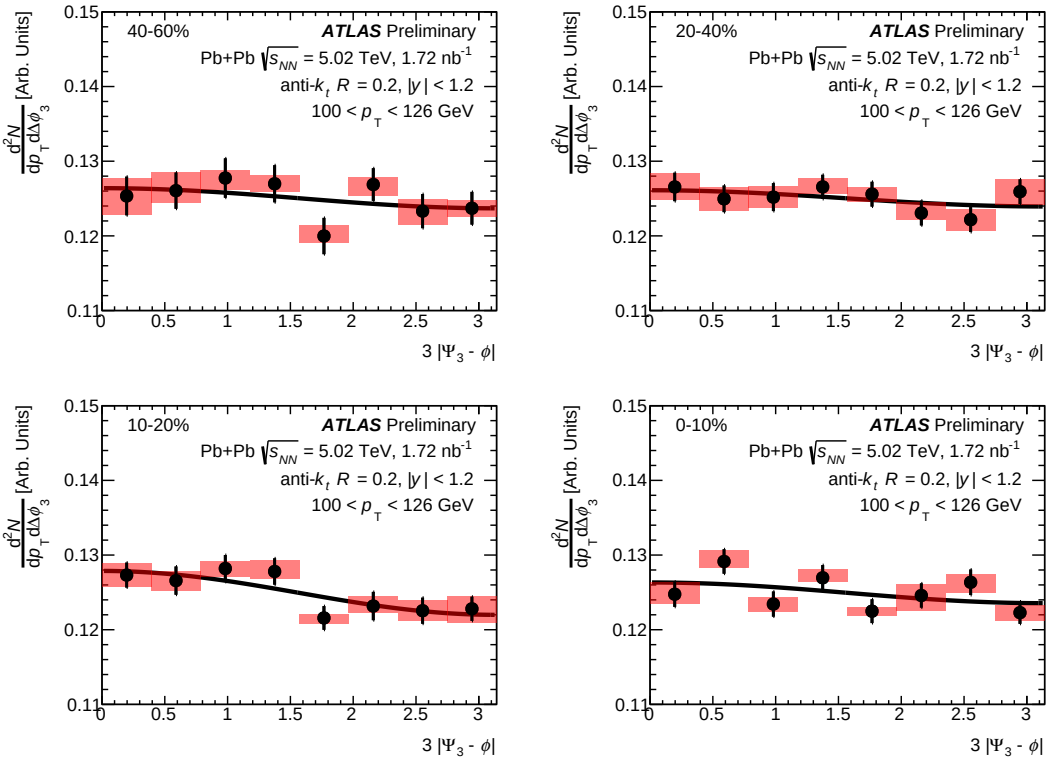

Figure 4: Angular distribution of jets with respect to the Ψ_3 plane for jets with $100 < p_{\mathrm{T}} < 126$ GeV for (from top left): 40–60%, 20–40%, 10–20%, and 0–10% central Pb+Pb collisions. The vertical bars show the statistical uncertainties and the boxes show the systematic uncertainties. The fits are to the function in Eq. 3.

in this analysis, while the ALICE measurement uses jets comprised of charged particle constituents (not including calorimeter information). However, this difference does not provide a natural explanation for the larger v_2 values in Ref. [10]. The comparison to charged-particle v_2 values from CMS [11] is also shown. At large transverse momentum, charged-particles are expected to come dominantly from jet fragmentation and thus the v_2 and v_3 values of the charged-particles are expected to originate from jets at higher transverse momentum. Due to the weak p_{T} dependence observed in the jet v_n it is expected that the charged-particle v_n should be consistent with this measurement. No significant difference is observed between the ATLAS jet v_2 values and the charged-particle v_2 values from CMS for both the 0–10% and 20–40% central collisions.

Figure 8 shows a comparison of the jet v_3 values measured here with those in charged-particles from CMS [11]. The CMS charged-particle v_3 measurements are in agreement with the jet anisotropies measured in this analysis. Both the jet and charged-particle v_3 show a lack of a strong transverse momentum dependence to the measured anisotropies. The v_3 values are consistent with zero.

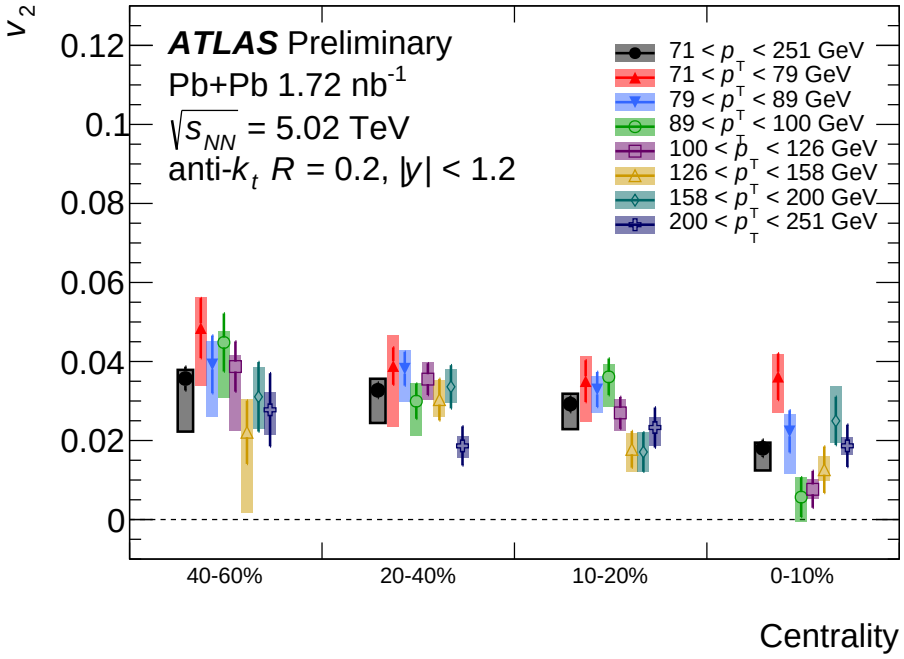

Figure 5: The v_2 values for $R = 0.2$ jets as a function of centrality for jets with p_T = 71–251 GeV. The vertical bars include the statistical uncertainty from the fits and the uncertainties from the response matrix statistics. The boxes represent the systematic uncertainties.

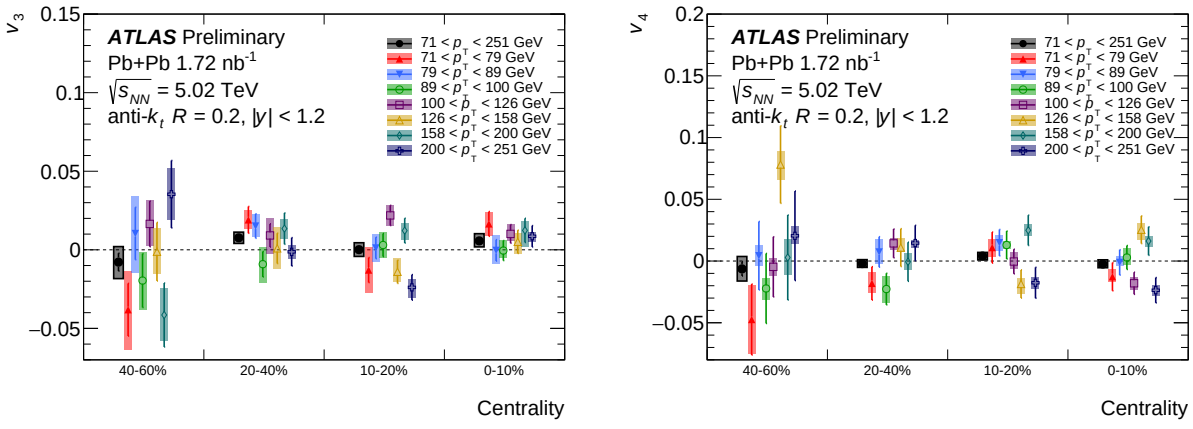

Figure 6: The v_3 (left panel) and v_4 (right panel) of $R = 0.2$ jets as a function of centrality for jets with p_T = 71–251 GeV. The vertical bars include the statistical uncertainty from the fits and the uncertainties from the response matrix statistics. The boxes represent the systematic uncertainties.

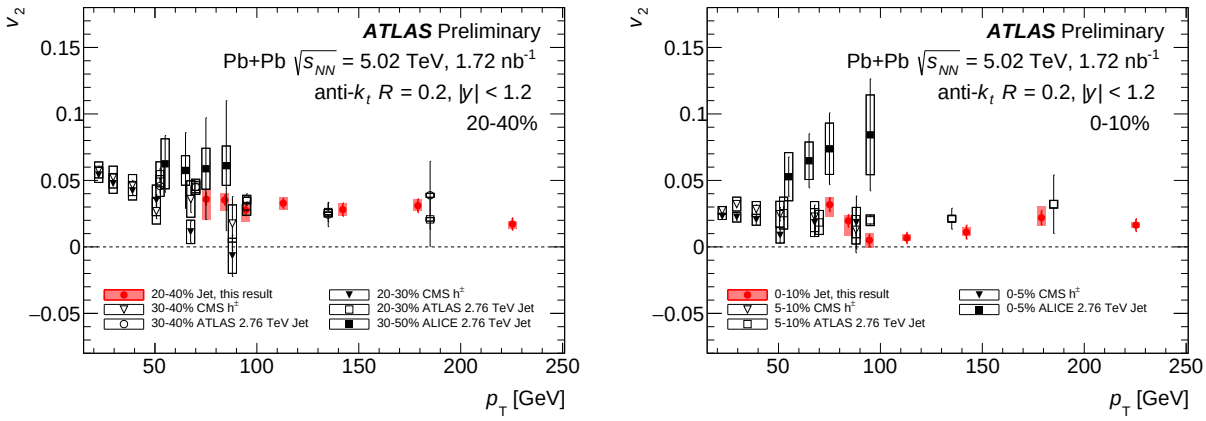

Figure 7: The v_2 as a function of p_{T} for jets in 20–40% (left) and 0–10% (right) collisions in this measurement (red circle) compared to the v_2 of jets in $\sqrt{s_{\mathrm{NN}}}$ = 2.76 TeV Pb+Pb collisions from Ref. [9] (open squares) and from Ref. [10] (black squares). Also shown are v_2 results for charged particles from CMS [11]. Note that the centrality ranges are slightly different between the four measurements.

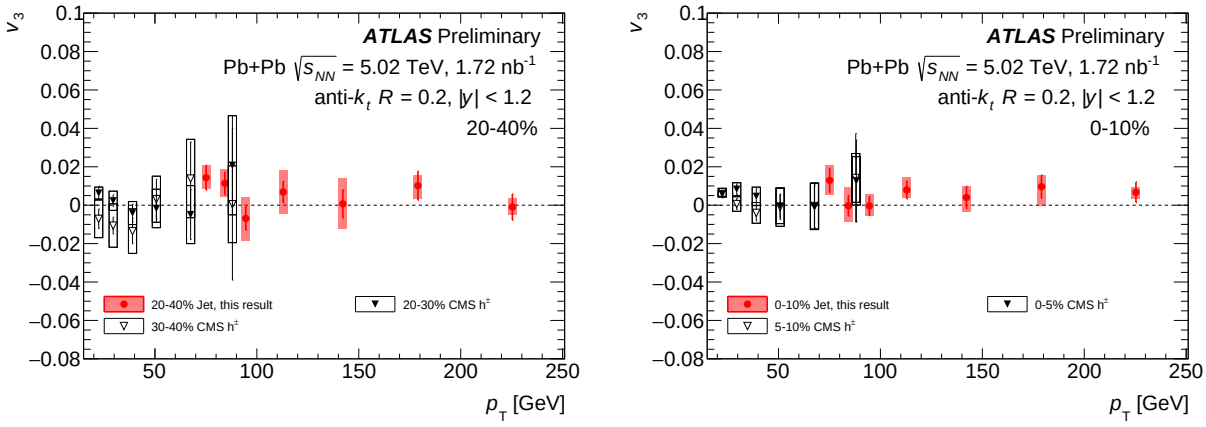

Figure 8: The v_3 values as a function of p_{T} for jets in 20–40% (left) and 0–10% (right) collisions in this measurement compared to charged particles in $\sqrt{s_{\mathrm{NN}}}$ = 5.02 TeV Pb+Pb collisions from Ref. [11]. Note that the centrality ranges are slightly different between the two measurements.

7 Conclusion

This note presents the first measurements of jet v_2, v_3, and v_4 in $\sqrt{s_{\mathrm{NN}}}$ = 5.02 TeV Pb+Pb collisions. The v_2 values are found to be positive and show no significant centrality or jet transverse momentum dependence within the uncertainties, however the result is also consistent with a possible decreased v_2 in the most central collisions as was seen in the previous ATLAS measurement [9] and is expected from collision geometry. The v_2 values are approximately 1–5%. The v_3 and v_4 values are found to be consistent with zero in all centrality and p_{T} measurements presented here. These anisotropies are qualitatively in agreement with those from high-transverse momentum charged particles [11]. The jet v_2 results are consistent with previous measurements at 2.76 TeV from ATLAS [9] and are lower than those from ALICE [10] in the most central Pb+Pb collisions. These measurements provide new information on the path-length dependence of jet quenching in Pb+Pb collisions.

References

[1] W. Busza, K. Rajagopal and W. van der Schee, *Heavy Ion Collisions: The Big Picture, and the Big Questions*, Ann. Rev. Nucl. Part. Sci. **68** (2018) 339, arXiv: 1802.04801 [hep-ph] (cit. on p. 2).

[2] ATLAS Collaboration, *Measurement of the nuclear modification factor for inclusive jets in Pb+Pb collisions at* $\sqrt{s_{\mathrm{NN}}}$ = 5.02 *TeV with the ATLAS detector*, Phys. Lett. **B790** (2019) 108, arXiv: 1805.05635 [nucl-ex] (cit. on pp. 2, 4).

[3] X.-N. Wang, *Jet quenching and azimuthal anisotropy of large p(T) spectra in noncentral high-energy heavy ion collisions*, Phys. Rev. C **63** (2001) 054902, arXiv: nucl-th/0009019 (cit. on p. 2).

[4] M. Gyulassy, I. Vitev and X. Wang, *High p(T) azimuthal asymmetry in noncentral A+A at RHIC*, Phys. Rev. Lett. **86** (2001) 2537, arXiv: nucl-th/0012092 (cit. on p. 2).

[5] E. Shuryak, *The Azimuthal asymmetry at large p(t) seem to be too large for a 'jet quenching'*, Phys. Rev. C **66** (2002) 027902, arXiv: nucl-th/0112042 (cit. on p. 2).

[6] J. Noronha-Hostler, B. Betz, J. Noronha and M. Gyulassy, *Event-by-event hydrodynamics + jet energy loss: A solution to the* $R_{AA} \otimes v_2$ *puzzle*, Phys. Rev. Lett. **116** (2016) 252301, arXiv: 1602.03788 [nucl-th] (cit. on p. 2).

[7] B. Betz et al., *Cumulants and nonlinear response of high* p_T *harmonic flow at* $\sqrt{s_{NN}}$ = 5.02 *TeV*, Phys. Rev. C **95** (2017) 044901, arXiv: 1609.05171 [nucl-th] (cit. on p. 2).

[8] U. Heinz and R. Snellings, *Collective flow and viscosity in relativistic heavy-ion collisions*, Ann. Rev. Nucl. Part. Sci. **63** (2013) 123, arXiv: 1301.2826 [nucl-th] (cit. on p. 2).

[9] ATLAS Collaboration, *Measurement of the Azimuthal Angle Dependence of Inclusive Jet Yields in Pb+Pb Collisions at* $\sqrt{s_{NN}}$ = *2.76 TeV with the ATLAS detector*, Phys. Rev. Lett. **111** (2013) 152301, arXiv: 1306.6469 [hep-ex] (cit. on pp. 2, 4, 5, 9, 12, 13).

[10] ALICE Collaboration, *Azimuthal anisotropy of charged jet production in* $\sqrt{s_{NN}}$=*2.76 TeV Pb+Pb collisions*, Physics Letters B **753** (2016) 511, ISSN: 0370-2693, URL: http://dx.doi.org/10.1016/j.physletb.2015.12.047 (cit. on pp. 2, 9, 10, 12, 13).

[11] CMS Collaboration, *Azimuthal anisotropy of charged particles with transverse momentum up to 100 GeV/ c in PbPb collisions at* $\sqrt{s_{NN}}$=*5.02 TeV*, Phys. Lett. **B776** (2018) 195, arXiv: 1702.00630 [hep-ex] (cit. on pp. 2, 10, 12, 13).

[12] ATLAS Collaboration, *Measurement of the azimuthal anisotropy of charged particles produced in $\sqrt{s_{NN}} = 5.02$ TeV Pb+Pb collisions with the ATLAS detector*, Eur. Phys. J. **C78** (2018) 997, arXiv: 1808.03951 [nucl-ex] (cit. on pp. 2, 4, 5).

[13] M. Cacciari, G. P. Salam and G. Soyez, *The anti-k_t jet clustering algorithm*, JHEP **04** (2008) 063, arXiv: 0802.1189 [hep-ph] (cit. on pp. 3, 4).

[14] ATLAS Collaboration, *The ATLAS Experiment at the CERN Large Hadron Collider*, JINST **3** (2008) S08003 (cit. on p. 3).

[15] M. Capeans et al., *ATLAS Insertable B-Layer Technical Design Report*, tech. rep. CERN-LHCC-2010-013. ATLAS-TDR-19, 2010, URL: https://cds.cern.ch/record/1291633 (cit. on p. 3).

[16] ATLAS Collaboration, *ATLAS Insertable B-Layer Technical Design Report Addendum*, tech. rep. CERN-LHCC-2012-009. ATLAS-TDR-19-ADD-1, Addendum to CERN-LHCC-2010-013, ATLAS-TDR-019, 2012, URL: https://cds.cern.ch/record/1451888 (cit. on p. 3).

[17] ATLAS Collaboration, *Trigger Menu in 2018*, ATL-DAQ-PUB-2019-001, 2019, URL: https://cds.cern.ch/record/2693402 (cit. on p. 4).

[18] ATLAS Collaboration, *Measurement of longitudinal flow decorrelations in Pb+Pb collisions at $\sqrt{s_{NN}} = 2.76$ and 5.02 TeV with the ATLAS detector*, Eur. Phys. J. **C78** (2018) 142, arXiv: 1709.02301 [nucl-ex] (cit. on p. 4).

[19] S. Agostinelli et al., *GEANT4—a simulation toolkit*, Nucl. Instrum. Meth. A **506** (2003) 250 (cit. on p. 4).

[20] ATLAS Collaboration, *The ATLAS Simulation Infrastructure*, Eur. Phys. J. C **70** (2010) 823, arXiv: 1005.4568 [physics.ins-det] (cit. on p. 4).

[21] ATLAS Collaboration, ATLAS-PHYS-PUB-2014-021, https://cds.cern.ch/record/1966419 (cit. on p. 4).

[22] R. D. Ball et al., *Parton distributions with LHC data*, Nucl. Phys. B **867** (2013) 244, arXiv: 1207.1303 [hep-ph] (cit. on p. 4).

[23] M. Cacciari, G. P. Salam and G. Soyez, *FastJet user manual*, Eur.Phys.J. **C72** (2012) 1896, arXiv: 1111.6097 [hep-ph] (cit. on p. 4).

[24] ATLAS Collaboration, *Jet energy measurement with the ATLAS detector in proton–proton collisions at $\sqrt{s} = 7$ TeV*, Eur. Phys. J. C **73** (2013) 2304, arXiv: 1112.6426 [hep-ex] (cit. on p. 4).

[25] ATLAS Collaboration, *Measurement of the azimuthal anisotropy of charged particles produced in $\sqrt{s_{NN}} = 5.02$ TeV Pb+Pb collisions with the ATLAS detector*, Eur. Phys. J. C **78** (2018) 997, arXiv: 1808.03951 [hep-ex] (cit. on p. 4).

[26] ATLAS Collaboration, *Jet energy measurement and its systematic uncertainty in proton-proton collisions at $\sqrt{s} = 7$ TeV with the ATLAS detector*, Eur. Phys. J. C **75** (2015) 17, arXiv: 1406.0076 [hep-ex] (cit. on p. 5).

[27] ATLAS Collaboration, *Measurement of photon-jet transverse momentum correlations in 5.02 TeV Pb+Pb and pp collisions with ATLAS*, Phys. Lett. B **789** (2019) 167, arXiv: 1809.07280 [hep-ex] (cit. on p. 5).

[28] ATLAS Collaboration, *Jet energy scale and its uncertainty for jets reconstructed using the ATLAS heavy ion jet algorithm*, ATLAS-CONF-2015-016, 2015, URL: https://cds.cern.ch/record/2008677 (cit. on pp. 5, 7).

[29] ATLAS Collaboration, *Measurement of azimuthal anisotropy of muons from charm and bottom hadrons in Pb+Pb collisions at $\sqrt{s_{NN}}$ = 5.02 TeV with the ATLAS detector*, (2020), arXiv: 2003.03565 [nucl-ex] (cit. on pp. 5, 7).

[30] A. M. Poskanzer and S. A. Voloshin, *Methods for analyzing anisotropic flow in relativistic nuclear collisions*, Phys. Rev. C **58** (3 1998) 1671, URL: https://link.aps.org/doi/10.1103/PhysRevC.58.1671 (cit. on p. 5).

[31] G. D'Agostini, *A Multidimensional unfolding method based on Bayes' theorem*, Nucl. Instrum. Meth. **A362** (1995) 487 (cit. on p. 5).

[32] T. Adye, 'Unfolding algorithms and tests using RooUnfold', *Proceedings, PHYSTAT 2011 Workshop on Statistical Issues Related to Discovery Claims in Search Experiments and Unfolding, CERN,Geneva, Switzerland 17-20 January 2011*, CERN, CERN, 2011 313, arXiv: 1105.1160 [physics.data-an] (cit. on p. 5).

[33] ATLAS Collaboration, *Jet energy measurement with the ATLAS detector in proton-proton collisions at $\sqrt{s}$ = 7 TeV*, Eur. Phys. J. C **73** (2013) 2304, arXiv: 1112.6426 [hep-ex] (cit. on p. 7).

[34] ATLAS Collaboration, *Jet energy scale measurements and their systematic uncertainties in proton-proton collisions at $\sqrt{s}$ = 13 TeV with the ATLAS detector*, Phys. Rev. D **96** (2017) 072002, arXiv: 1703.09665 [hep-ex] (cit. on p. 7).

[35] ATLAS Collaboration, *Jet energy resolution in proton-proton collisions at $\sqrt{s}$ = 7 TeV recorded in 2010 with the ATLAS detector*, Eur. Phys. J. C **73** (2013) 2306, arXiv: 1210.6210 [hep-ex] (cit. on p. 7).

[36] ATLAS Collaboration, *Determination of jet calibration and energy resolution in proton-proton collisions at $\sqrt{s}$ = 8 TeV using the ATLAS detector*, (2019), arXiv: 1910.04482 [hep-ex] (cit. on p. 7).